



**HAL**  
open science

## Nanocomposite powder for powder-bed-based additive manufacturing obtained by dry particle coating

Mathieu Soulier, A. Benayad, L. Teulon, Y. Oudart, S. Senol, K. Vanmeensel

### ► To cite this version:

Mathieu Soulier, A. Benayad, L. Teulon, Y. Oudart, S. Senol, et al.. Nanocomposite powder for powder-bed-based additive manufacturing obtained by dry particle coating. Powder Technology, 2022, 404, pp.117474. 10.1016/j.powtec.2022.117474 . cea-03764332

**HAL Id: cea-03764332**

**<https://cea.hal.science/cea-03764332>**

Submitted on 30 Aug 2022

**HAL** is a multi-disciplinary open access archive for the deposit and dissemination of scientific research documents, whether they are published or not. The documents may come from teaching and research institutions in France or abroad, or from public or private research centers.

L'archive ouverte pluridisciplinaire **HAL**, est destinée au dépôt et à la diffusion de documents scientifiques de niveau recherche, publiés ou non, émanant des établissements d'enseignement et de recherche français ou étrangers, des laboratoires publics ou privés.

# NANOCOMPOSITE POWDER FOR POWDER-BED-BASED ADDITIVE MANUFACTURING OBTAINED BY DRY PARTICLE COATING

Soulier, M.<sup>a</sup>, Benayad, A.<sup>a</sup>, Teulon, L.<sup>b</sup>, Oudart, Y.<sup>b</sup>, Senol, S.<sup>c</sup>, Vanmeensel K.<sup>c</sup>

<sup>a</sup> Univ. Grenoble Alpes, CEA, Liten, DTNM, 38000 Grenoble, France

5 <sup>b</sup> Nanomakers, 1 rue de Clairefontaine, Rambouillet, 78120, France

<sup>c</sup> Department of Materials Engineering, KU Leuven, 3001 Leuven, Belgium

**Keywords: Dry coating, Powder functionalization, Electrostatic assembly, Additive manufacturing, Powder spreading, Nanoparticles.**

10 DOI

<https://doi.org/10.1016/j.powtec.2022.117474>

## 1. Introduction:

15 Powder bed based (PBB) additive manufacturing (AM) such as laser powder bed fusion (L-PBF) [1] or Binder Jetting (BJ) [2] constitute a hot spot for academic and industrial research to produce near net shaped parts with complex geometries. These technologies have the potential to disrupt conventional manufacturing techniques such as stir casting or welding by enabling lightening and multi-functional components.

20 PBB-AM techniques are based on the spreading of thin layers of powders intended to be either selectively melted by a laser (L-PBF) or bound together through a printer head (BJ). The processed powders have to meet stringent specifications. The challenge is made more complex as powder requirements are influenced by the device used to spread powder layers (typically rake or a rotating roller) and by the powder feeding system (piston or hopper) [3].

25 Particle shape and size are particularly important in PBB-AM since they affect interparticle friction forces and, as a consequence, particle packing (i.e. powder bed density) [4] [5] [6] [7] [8] and powder flowability in the feeding system [9] [10]. In the L-PBF process for example, the use of irregular particles' shapes increases the required laser energy to obtain fully dense parts [11] and may lead to the presence of residual porosities after printing [12] and higher part roughness [13]. In BJ process, the powder packing criterion is even more important since the mechanical strength of the printed green part is directly linked to the powder bed apparent density [2].

30 In this context, new developments related to Metal Matrix Composite (MMCs) are emerging in PBB – AM processes and stir casting [14] [15]. One main ambition is to address new applications for automotive and aerospace industries by improving specific strength, stiffness or wear resistance of commonly printed metal materials (inconel, stainless steel, aluminium, titanium alloys), especially by adding ceramic reinforcements like Al<sub>2</sub>O<sub>3</sub>, B<sub>4</sub>C, TiB<sub>2</sub>, SiC, TiC, Y<sub>2</sub>O<sub>3</sub> [2] [11] [14] [16] [17] [18] [19]. Most of this new class of materials are embedding nanoscale reinforcements. In these so-called Metal Matrix nano-Composites (MMnCs), nano sized reinforcements serve to multiply interactions between reinforcements and dislocations resulting in a higher improvement of mechanical properties [20] [21].

40 Another promising perspective of MMnCs in PBB is the addition of nanosized nucleating agents to the starting metal powder in order to avoid hot cracking occurring in a number of high performance alloys (such as 6000 and 7000 series aluminium or nickel superalloys) [22] [23]. This approach allows a control of the solidification microstructure, promoting fine equiaxed grain microstructure and avoiding the formation of large columnar grains sensitive to hot tearing.

45

In BJ, the addition of nanoparticles within the powder bed is studied to improve the sinterability (nanoparticles sinter at lower temperature) and to reduce shrinkage [2].

50 If developments of MMnCs for PBB-AM processes are very promising, they are still in their infancy and face issues to elaborate suitable powder composite mixtures (usually guest nanopowders on top of host micrometric metallic powders). Indeed, the nanocomposite powders have to satisfy common PBB-AM powder specifications (good spreadability, flowability and stability during spreading) while using nanoparticles has a strong impact on the composite powder behavior [22]. Indeed, Van der Waals forces between nanoparticles are prevailing over their respective weights, often resulting in  
55 poor flowability [24] [25] [26] and stacking defects in powder layers [27].

The most common procedure to generate nanocomposite powder dedicated to additive manufacturing is ball milling in a dry state [16]. The powder mixture is subjected to ball collisions in a rotating jar, creating repeated welding, fracturing and rewelding of powders [11] [17]. This technique enables the control of the particle size down to the sub-micrometric scale and the synthesis of a variety  
60 of non-equilibrium phases. However ball milling is also prone to potential powder contamination by the milling media and milled powders are generally more sensitive to oxidation and pyrophoricity [16] [28]. In addition, ball milling is degrading the shape of the starting powders, which impacts the packing density with respect to the initially spherical powders.

As a comparison, many reports in the food and pharmaceutical literature have demonstrated the  
65 improvement of powder flowability and packing by dispersing “guest” particles among “host particles” through high-shear mixing methods [29]-[36]. The principle, commonly called dry coating, is to self-assemble guest nanoparticles by triboelectricity at the surface of host particles via electron transfers between the two types of powders (*Figure 1*). Dry coating is achieved by various mixing technologies as paddle mixer, acoustic mixer, mechanofusion, Magnetic Assisted Coating (MAIC) or Hybridizer  
70 coating (HB). Compared to ball milling, dry coating aims to obtain stable powder mixtures without high deformation of particles to target high flowability and packing behaviours. The process presents the benefit of being cost effective, solvent free and energy efficient, as it does not require a drying step [29].

75



Interactive mixture

80 *Figure 1: Schematic of an interactive powder mixture obtained by electrostatic self-assembly.*

Within this context, we study the potential of dry particle coating to prepare metallic nanocomposite powder for PBB-AM processes. Different mixing techniques are assessed from laboratory scale to industrial scale to achieve the dry coating of aluminium powders by nanosized silicon carbide particles.  
85 The ultimate goal is to be able to print these functionalized nanocomposite powders to achieve ceramic reinforcement of the base aluminium alloy. The present work proposes a thorough characterization of the nanocomposite powders. More precisely, coating performances and powder mixture properties are evaluated as well as nanocomposite powder behaviors (flowability, optical reflectivity, apparent density, host particle shape). The oxidation state of starting guest particles on  
90 dry coating efficiency is lastly assessed.

## 2. Materials and methods

### 2.1 Powders

#### Aluminium host powder

95 The host powder is a 15-53 $\mu$ m aluminium alloy AS7G06 (AlSi<sub>7</sub>Mg<sub>0.6</sub>) supplied by TLS Technik GmbH & Co and produced by nitrogen gas atomisation. This aluminium-silicon hypo-eutectic alloy is commonly used in L-PBF processes to produce aluminium parts because of its low tendency of hot-tearing. The detailed chemical composition is presented in *Table 1*.

	Al	Si	Mg	Ti	Fe	Zn	Mn	Cu
AS7G06 gas atomized powder	Bal.	7.23	0.62	0.18	0.18	≤ 0.001	≤ 0.003	0.005

*Table 1: Chemical composition of the AlSi<sub>7</sub>Mg<sub>0.6</sub> powder used as the matrix alloy (wt%).*

100

#### Silicon carbide guest nanopowder

Silicon carbide (from Nanomakers) is used as guest nanoparticles for dry coating. SiC nanoparticles are synthesized by laser pyrolysis of two gaseous precursors, silane (SiH<sub>4</sub>) and acetylene (C<sub>2</sub>H<sub>2</sub>) as described in (patent FR2894493B1). Briefly, a CO<sub>2</sub> laser radiation is absorbed by silane and transferred to acetylene which leads to molecular dissociation and nanopowders production through a nucleation and growth process.

105

The SiC nanoparticles possess well-defined properties thanks to an accurate control of the synthesis parameters such as the gaseous precursors concentrations, their flow rates and the laser power. The laser activation enables very fast and controlled temperature increases.

110

SiC guest nanoparticles have a specific surface area according to BET (Braunet Emmet Teller) measurement of 55.6 ± 0.6 m<sup>2</sup>/g.

SiC nanoparticles are granulated through a dry rotative mechanical process (CEA patent EP2648834B1) to form particles agglomerates of few millimeters in diameter, easier to handle than the standard loose powder. These agglomerates are brittle and easily broken at the beginning of the mixing process.

115

### 2.2 Dry coating processes

Four different dry mixing routes were assessed to prepare the nanocomposite powders.

120

(1) Tridimensional rotative drum mixer:

A dry mixing procedure was developed using a laboratory scale tridimensional shaker mixer (Turbula, T10B model, presented in *Figure 2*) to prepare nanocomposite powder batches of 0.7 Liter. The drum is filled with the host and guest powders, which are then subjected to blending resulting from the periodic translational and rotational movements of the container. The rotative drum mixer based on convection modes of mixing is inoperative if no grinding balls are incorporated in the vessel to reduce the scale of powder rearrangement, initially proportional to the drum size. Grinding balls media have to be added in the vessel to apply shear forces on the powders and reduce the extent of powder rearrangement in the vessel. Thanks to a high filling rate, grinding balls roll against each other and are thus able to break the agglomerates of cohesive nanoparticles.

125

130



Figure 2: Schematic of the Turbula motion wherein powders are subjected to periodic translational and rotational movements to achieve blending (Schematic source: <https://aerosol-soc.com/wp-content/uploads/2016/06/1500-Hertel-Pent-Thurs-v1.pdf>).

135

(2) High shear paddle mixer:

An industrial high shear mixer of 50 Liters has been tested to dry coat the aluminium powder. The static conical shaped mixer is equipped by an axial impeller with five pairs of paddles, three of which are applying high shear forces against the inner wall of the vessel (Figure 3). The paddles tangential velocity is adjustable from 3 to 30 m/s.

140

While rotating, the product is pushed outwards due to the centrifugal forces, then the product is pushed upwards due to the angle in the vessel and downwards again due to the shape of the vessel cover. At the top of the vessel, the knife blades (removable) generate impact forces in order to de-agglomerate the product if necessary.

145

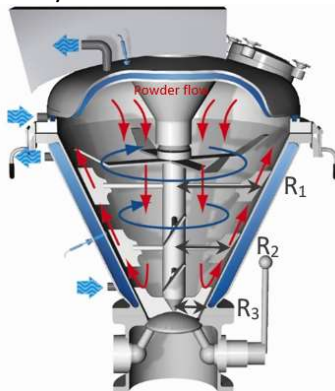


Figure 3: High shear conical paddle mixer developed by Hosokawa marketed under the name Cyclomix (schematic source: OndrugDel. 85 (2018) 48-49)

150

(3) Low shear helices mixer:

The tested low shear mixer is a 20 Liters cylindrical vessel mixer equipped by two vertical mixing tools, twisted in an helicoidal pattern (Figure 4). The rotational velocity is significantly lower compared to the high shear mixer (adjustable from 0.8 m/s to 3.5 m/s). This range of operating speed is corresponding to a gentle mixing. A speed of 2 m/s was set for this study. An additional chopper (cutting rotor) rotating at 3 m/s is embedded at the bottom of the vessel to break powder agglomerates during mixing.

155



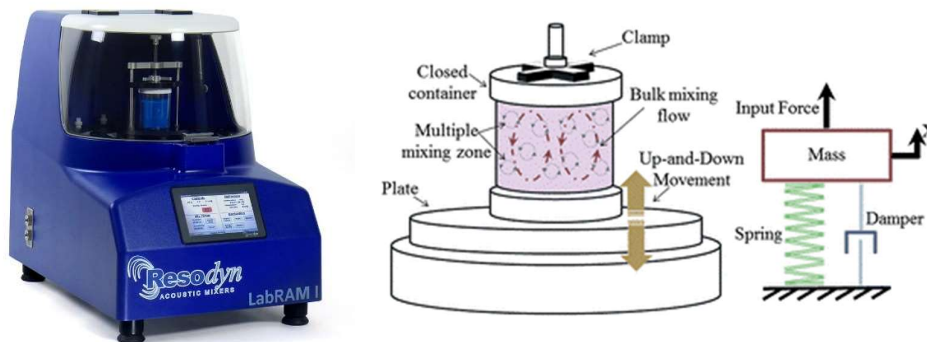
Figure 4: Twin-helices mixer (<https://www.amixon.com/en/products/vertical-twin-shaft-mixer>)

160

(4) Acoustic mixer:

A low-frequency acoustic mixer has also been tested to prepare 200 mL batches of dry coated powders (Figure 5). This impeller-free mixing technology induces microscale turbulence in the powder mixture through the propagation of acoustic waves. The acoustic waves submit the powder to strong accelerations through vertical motions of the container, thus achieving powder blending [37]. The acceleration can be set up from 10 g to 100 g generating intense powder motions leading to numerous collisions between particles and micro-shear in the powder. In the present work, the evaluation of the dry coating ability was performed at 60 g to avoid product rise in temperature above 60°C.

165



170

Figure 5: Picture of Resodyn LabRAM1 equipment and schematic of the associated mixing mechanism (Picture source: <https://resodynmixers.com/product/labram-1/>, schematic source: RSC Adv. 6 (2016) 87049-87057).

175 Main equipment descriptions and operating conditions used in this study are reported in Table 2. Evaluated mixing apparatus are using different technologies and working with different impeller configurations/size. The resulting various level of impacts, shearing and friction, make difficult a direct comparison. However, the mixing systems can be in a first approach simplified to a characteristic velocity derived from the tip velocity of the impeller or vessel rotation speed. From this velocity, a kinetic energy per mass unit is calculated [38].

180

All mixing experiments were performed by filling the respective vessels with inert gas in glove box (O<sub>2</sub> and H<sub>2</sub>O content below 20 ppm) to limit the variation of environmental mixing conditions that affect the triboelectric charging [39] [40].

185 For all the tested coating processes, a complete electrostatic assembly of SiC nanoparticles is targeted. Indeed, an excess of guest particles in the powder would oversaturate the surface of the host powders. As a result the free fraction of guest nanoparticles dispersed in the mixture would increase the whole powder cohesivity and drastically impact the flowability [25] [26] [27] [33] [34].

Equipment	Characteristic dimensions (cm)	Vessel volume (L)	Mass of powder (kg)	Solid volume fraction (%)	Rotation frequency N (rpm)	Characteristic velocity V (m/s)	Characteristic energy E (J/kg)
Rotative drum mixer	R=19	17	0.97	32 by powder bed (67 powder + grinding balls)	32	$2\pi NR=0.6$	$\frac{v^2}{2} = 0.2$
High shear paddle mixer	R <sub>1</sub> =26 R <sub>2</sub> =18 R <sub>3</sub> =9	50	45	70	690	$2\pi N(\sum Ri/3)=12.8$	$\frac{\sum v_i^2}{3} = 84.5$
Low shear helices mixer	n.a	20	20	70	143	2 <sup>(1)</sup>	2
Acoustic mixer	R= 2.5	0.23	0.26	85	3600 (vibrations per minute)	$2\pi NR = 9.4$	$\frac{v^2}{2} = 44.4$

Table 2: Equipment descriptions and operating conditions.

(1) Manufacturer's data

190

### 2.3 Characterization

The coating of aluminium alloy particles is observed by Scanning Electron Microscopy (SEM). An automated particle image analysis (Malvern Morpho G3<sup>®</sup> morpho granulometer) is used to study the Particle Size Distributions (PSD) of the different powder mixtures to assess the coating efficiency. These measurements are performed under dry route after air pulverization on a glass plate of 11mm<sup>3</sup> of powder. Same procedure is also applied to nanocomposite powders to examine the host particle deformation during mixing. Thus, the particles aspect ratio, defined as the width to length ratio, is measured statistically on 50 000 particles/sample. Particle width and length are here defined thanks to Feret's diameter (ISO 9276-1).

200 Powder apparent and tap densities are determined on a Quantachrome Autotap<sup>TM</sup> analyzer using 250 mL of powder and 1000 taps (ISO 787/11). In addition, two phenomenological powder flow tests are performed; free-flowability is evaluated by avalanche angle method in a rotating drum at 0.6 rpm (Mercury Scientific Revolution<sup>®</sup>) and funnel flowability is assessed in Carney funnel test (standard B964). Powder mixture optical reflectivity is measured by a spectrophotometer (model Perkin Elmer, Lambda 950) in a wavelength range from 800 to 1200 nm. Finally, the surface and subsurface (say a few nm in range) chemistry of the composite powders is analyzed by X-ray photoelectron spectroscopy (XPS, PHI VersaProbe II).

## 3. Results and discussion

210 The purpose in this section is to evaluate the potential of different mixing processes to achieve dry coating of aluminium powder (host particles) by nanometric silicon carbide nanoparticles (guest particles). The efficiency of dry coating is studied following first the fraction of guest particles actually assembled and verifying the possible deformation of host particles during the mixing process. Afterwards, the modification of powder behavior by the coating is analyzed in terms of flowability, packing and optical reflectivity.

215

### 3.1 Characterization of starting powders

#### Aluminium host powder

Scanning Electron Microscopy (SEM) images of the aluminium alloy powder (*Figure 6*) emphasize the high sphericity of the individual particles permitted by the gas atomization process [41]. However, interparticle forces (Van der Waals and hydrogen weak bonds) lead to spontaneous formation of agglomerates. The *Table 3* presents the analysis of size, shape and true density of the aluminium primary particles. The average particle size characterized by automated image analysis after air dispersion is measured at 31 microns. The particle shape of aluminium powder has a median aspect ratio of 0.91, a value close to an aspect ratio of 1 qualifying a perfectly circular particle. The particle true density measured by helium pycnometry indicates that atomized particles are fully dense.

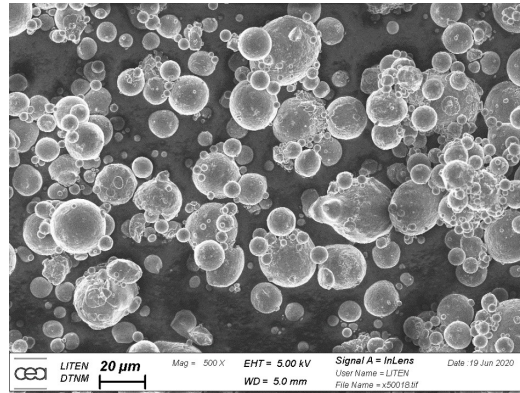


*Figure 6: Scanning electron microscopy (SEM) image of the matrix powder: AlSi7Mg0.6.*

	Particle size distribution (D10/D50/D90) <i>By automated image analysis</i>	Median particle aspect ratio (D50) <i>By automated image analysis</i>	True density <i>By Helium pycnometry</i>	Moisture content <i>By Karl Fisher titration</i>
AS7G06 gas atomized power	Vol. %: 17 / 31 / 50 $\mu\text{m}$ Nbr. %: 6 / 15 / 29 $\mu\text{m}$	0.91 $\pm$ 0.02	2,6587 $\pm$ 0,0003 g/cm <sup>3</sup>	130 ppm

*Table 3: Particle size distribution, particle morphology (aspect ratio), true density and moisture content of the starting 15-53 $\mu\text{m}$  AS7G06 powder.*

#### Silicon carbide guest nanopowder

A Transmission Electron Microscopy (TEM) analysis of the nanoparticles is given in *Figure 7* showing their broadly spherical individual shapes and a specific chain-like arrangement. The nanoparticles present a 35nm average diameter with a narrow size distribution.

The starting SiC nanoparticles used for the study are dry granulated to be agglomerated in the form of brittle granules having a typical size between 0.1 and 2 mm, with an average granule size of 0.5mm estimated by sieving (*Figure 8*). The specific surface area of nanoparticles remain unchanged but the powder apparent density is widely increased from 0.005 g/cm<sup>3</sup> to 0.55 g/cm<sup>3</sup>, improving powder flowability and handling.

Assuming that host and guest particles are spherical in shape and monodisperse, *Yang et al.* provides an equation estimating the weight percentage of guest nanoparticles (*Gwt%*) to achieve a 100% surface area coverage of the host particles [30]:

$$Gwt\% = \frac{(Nd^3\rho_d)}{(D^3\rho_D)+(Nd^3\rho_d)} \times 100 \quad Eq. 1$$

With :

$$N = \frac{4(D+d)^2}{d^2} \quad Eq. 2$$

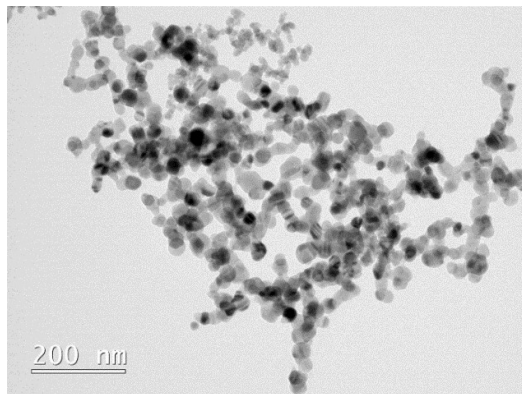
250 Where  $D$  and  $d$  are respectively the diameter of the host and guest particles,  $\rho_D$  and  $\rho_d$  their material densities.

From Eq. 1, the theoretical weight percentage to fully saturate the surface of 31  $\mu\text{m}$  aluminium powder with 35 nm silicon carbide nanoparticles aluminium is 0.5 wt.%.

Based on this approximate guideline, 1.0 wt.% of nanosized particles was used for the experimental study as this weight content is supposed to drastically improve aluminium mechanical properties [15].

255 Assuming all the guest particles to be uniformly assembled onto the surface of the aluminium particles, such a 1.0 wt.% amount corresponds to a theoretical thickness of 70 nm, or in average a stack of 2 layers of SiC nanoparticles .

260 In dry coating techniques, the reduction in the contact force due to the presence of small guest particles is inversely proportional to guest particle size [30]. The particle size of host particles is commonly selected to be 10 to 2000 times larger than guest particles. However, ratio higher or equal to 150 are preferred to improve drastically the host powder flowability [29]-[36]. In this study, the host to guest particle size ratio is 860, in a favorable range to perform dry coating while improving host particle rheology.



265 *Figure 7: Transmission electron microscopy (TEM) image of SiC nanoparticles.*

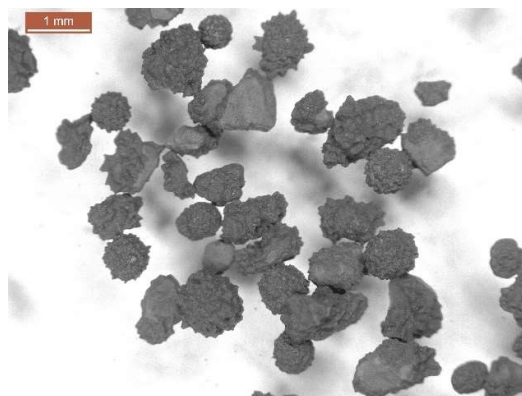


*Figure 8: Microscope picture of starting SiC granules.*

### 3.2 Assessment of dry coating processes

#### 3.2.1 Comparison of dry coating efficiency

Al-SiC nanocomposite powders are prepared by using the four mixing processes described in section 2.2.

Efficiency of the electrostatic assembly is evaluated by investigating the PSD expressed in number percentage of the powder mixtures using an automated image analysis at magnification X20. The number distribution (as opposed to volume) enables a sensitive identification of small SiC agglomerates remaining in the powder. Indeed, in the very first steps of mixing, the brittle SiC granules at millimetric scale (*Figure 8*) are expected to be divided into small agglomerates, and most of them becomes finer than host aluminium particles. Then uncoated Al/n-SiC powder mixture as analyzed by morphogranulometry appears bimodal; the aluminum powder peak is located centered at 20 microns, closed to the mean particle size reported in the *Table 3*. Another mode can be detected at that magnification, located between 1 and 5 microns and corresponding to uncoated SiC agglomerates. By contrast, a complete electrostatic assembly of SiC nanoparticles leads to a monomodal PSD, the only mode remaining being that of the host aluminium powder, testifying of the stability of the powder mixture (as represented in *Figure 1*). The study of the nanocomposite PSD according to the mixing operating time thus allows to establish the required mixing time for each process and to compare the coating efficiency between mixing technologies. As an example, the dry coating kinetics for the acoustic mixer are shown in *Figure 9*. After 7 minutes of mixing time, the PSD of mixed powders presents a peak between 1 and 4 microns which was not present on the initial aluminium powder. This signature indicates that a significant fraction of smalls SiC agglomerates is still not coated on the host powder surface. After 10-15 minutes, the PSD of the nanocomposite powder becomes similar to the PSD of the initial aluminium powder, showing an interactive mixture presented schematically in *Figure 1*.

The assessment of the dry coating assembly is completed by EDX elemental maps (*Figure 10*). These analyses are performed to detect in particular SiC agglomerates/granules remaining in the powder mixture that may have similar size as the aluminium particles and would not be detected by PSD analysis.

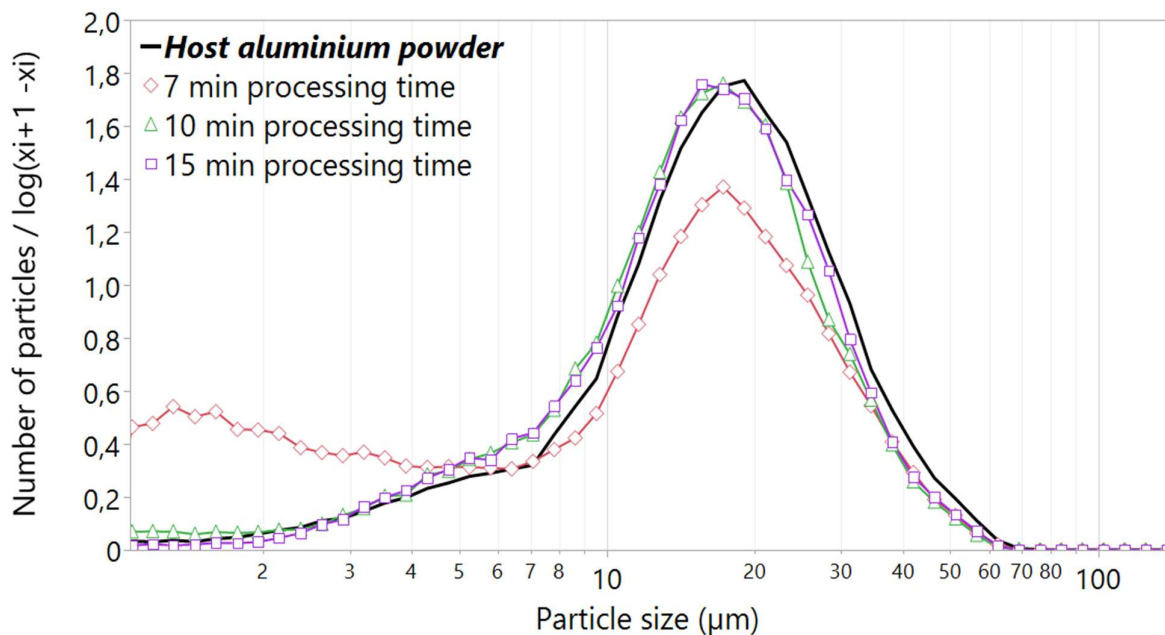


Figure 9: Evolution of the Al/1wt %n-SiC nanocomposite PSD using the acoustic mixer from 7 minutes to 15 minutes. PSD evaluations are performed by automated image analysis.

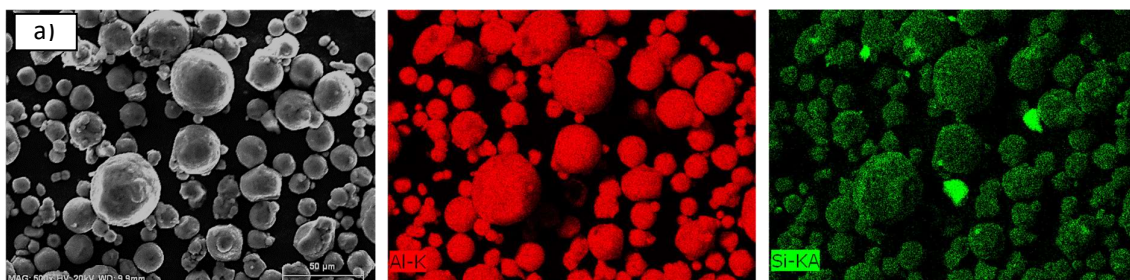
300 For each mixing technology, an optimization of the process duration requested to achieve complete assembly is carried out. The resulting optimal PSD are summarized in *Figure 11* and *Table 4*. The high shear paddle and the acoustic mixers, which are the two highest energy mixers in this study (*Table 2*), achieve a monomodal PSD within less than 15 minutes. The corresponding EDX element maps presented *Figure 10 (b, d)* shows no remaining SiC granules in the powder mixture.

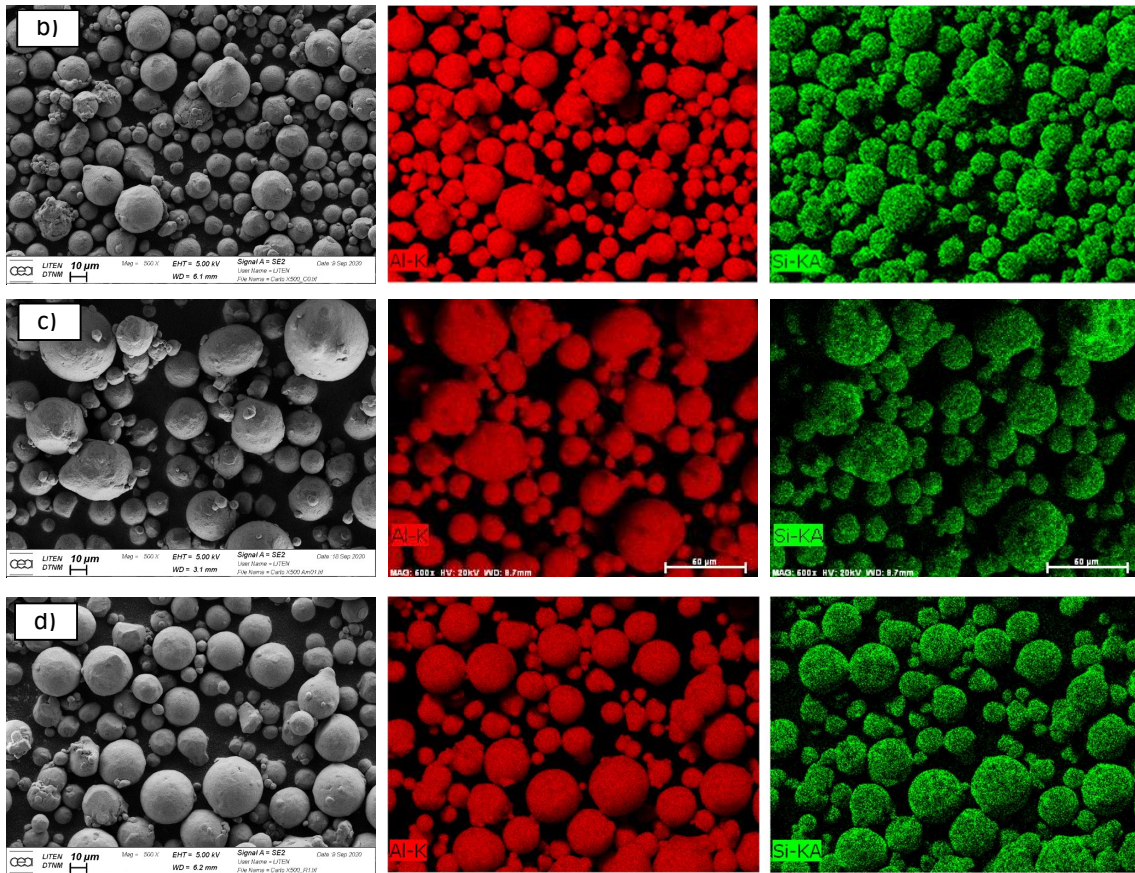
305 Both high shear paddle mixer and acoustic mixer lead to a complete adhesion of nanosized guest particles on the host aluminium particles, ensuring a fully interactive mixture. If coating performances are similar for these two mixers, it should be noted that their respective scales are widely different, that is a powder weight of 45 kg for the high shear paddle and 0.26 kg for the acoustic mixer. The *Figure 11* also reveals for the high shear paddle mixer a shifting to the left, towards smaller particle size, of the main peak assigned to aluminium powder. Two hypotheses could explain this change in size distribution. The first one is a fracturing or abrasion of the aluminium powder occurring during mixing. The second hypothesis is a less agglomerated state of the aluminium powder once coated. This point is addressed in the next section after the discussion on particle shape upon mixing.

310  
315 On the other hand, the lowest energy system tested, that is the rotative drum mixer, shows a remaining peak between 1 and 3 microns even after 8 hours of mixing. This peak is attributed to remaining fine agglomerates of SiC nanoparticles in the powder mixture. The EDX analysis *Figure 10 (a)* is highlighting the segregation of the guest particles in agglomerated form.

The intermediate energy mixer, that is the low shear helices mixer, reaches a monomodal PSD, comparable to higher energy mixers studied (*Figure 11*). However, starting SiC granules are still present in the powder mixture by SEM analysis as presented in *Figure 12*. The PSD expressed in number fraction does not highlight these big sized SiC granules (100 $\mu$ m-1mm) due to their low number. A sieving indicates that up to 30 wt.% of initially added SiC granules are still in granules form after 30 minutes of mixing. If the characteristic mixing energy of the low shear helices mixer is expected to be larger compared to the rotative drum mixer (*Table 2*), the high packing density of the grindings balls added in the latter (static grinding balls packing density measured at 0.69) allows to decrease the scale of particle-to-particle rearrangement in the vessel. Meanwhile, the tangential speed of 2m/s of the helices does not allow a sufficiently small scale of particle rearrangement to reduce efficiently in size the starting SiC granules. The use of an additional chopper rotating at 3 m/s at the bottom of the vessel does not increase enough the mixing energy to reverse this trend.

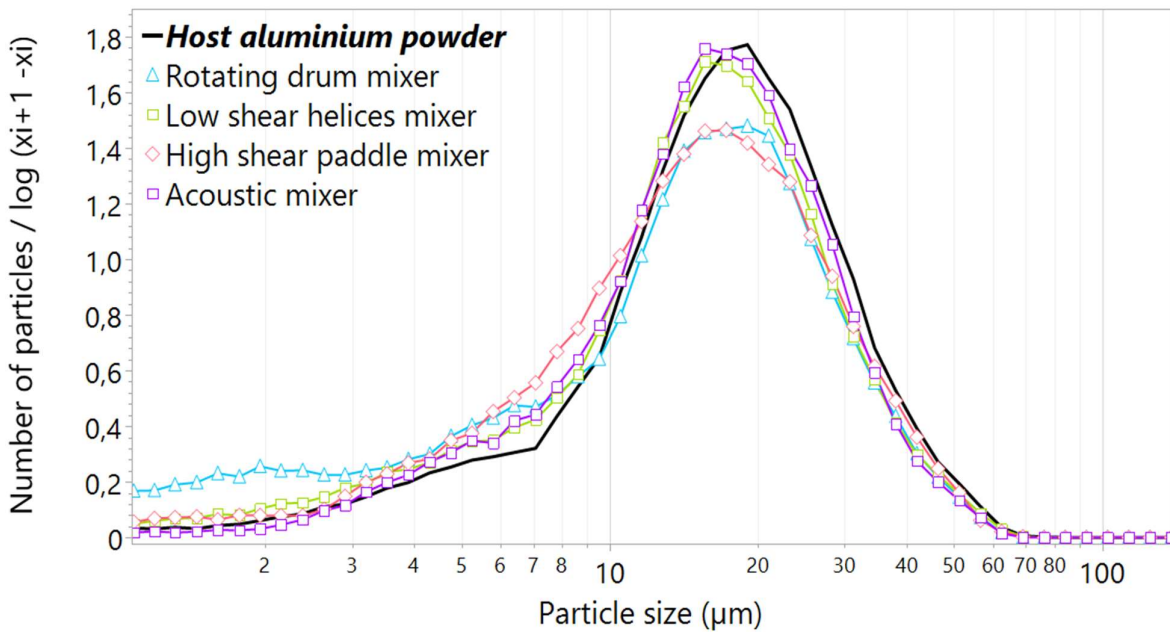
330





335

Figure 10: Secondary electron-SEM images (left) of the mixed powder and EDX elemental maps of Al (middle) and Si (right) for (a) rotating drum mixer; (b) high shear paddle mixer, (c) low shear helices mixer; (d) acoustic mixer.



340

Figure 11: Evaluation of the PSD of powder mixtures after optimization of processing time. PSD evaluations are performed by automated image analysis;

	Processing time to achieve interactive mixture
Rotative drum coated Al powder	7-8 hours (uncompleted)
High shear paddle coated Al powder	10-20 min
Low shear helices coated Al powder	30 min (uncompleted)
Acoustic coated Al powder	10-15 min

Table 4: Required processing time for each mixer to achieve an interactive mixture between host aluminium powder and guest silicon carbide nanoparticles.

345

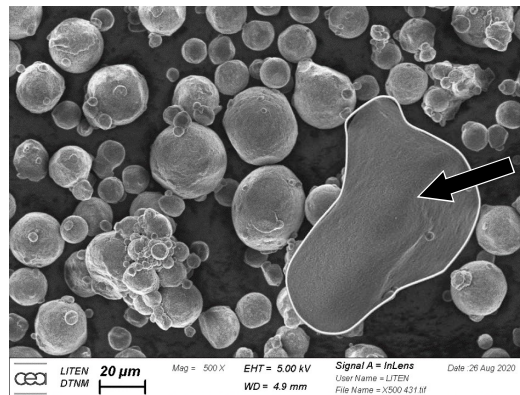


Figure 12: SEM images of low shear coated mixer pointing out a SiC agglomerate on the right.

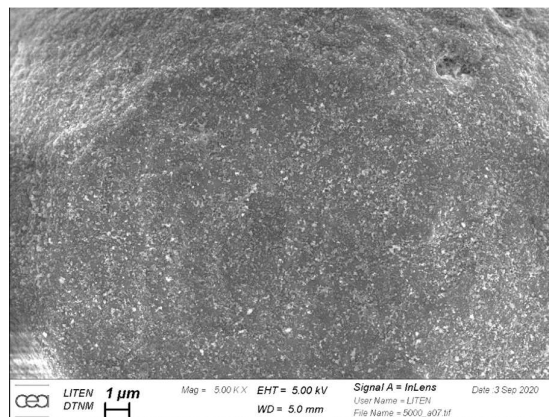
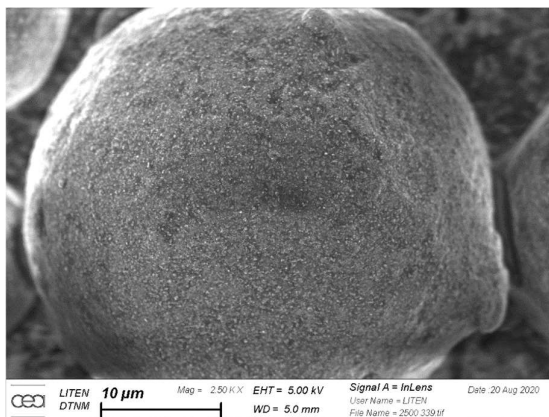
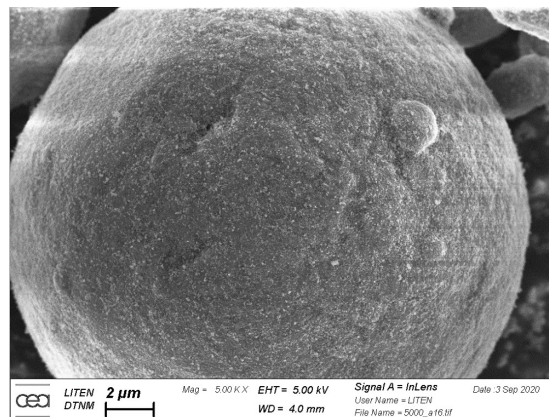
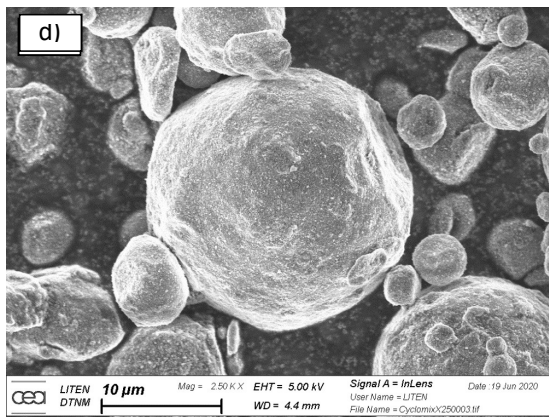
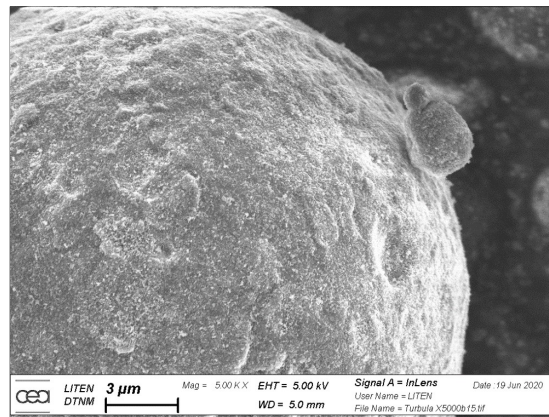
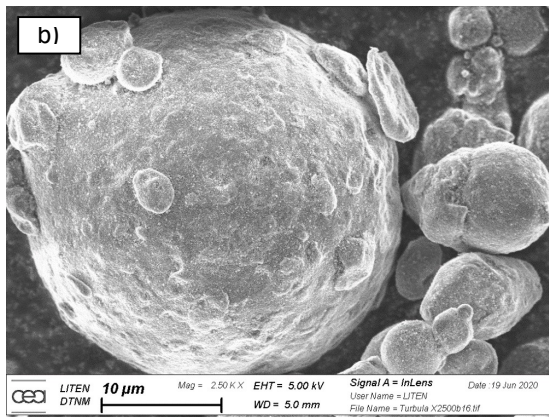
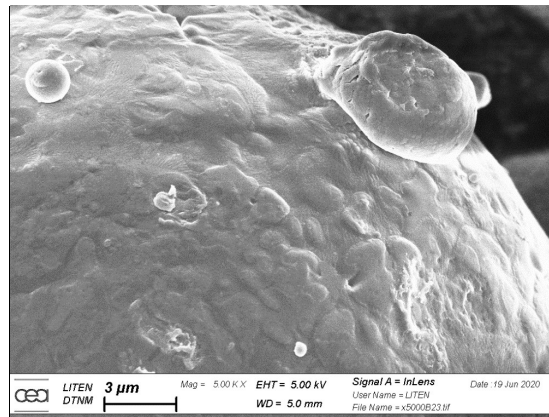
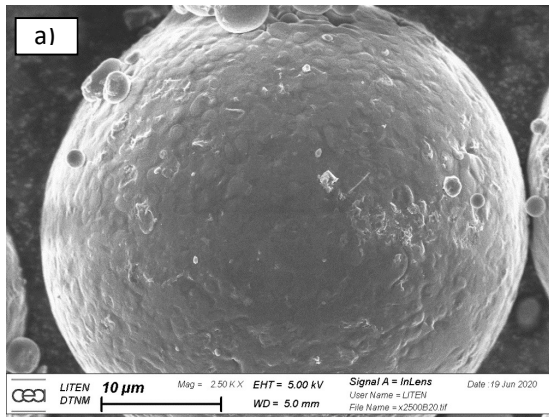
### 350 3.2.2 Surface characterizations and host powder morphology

The different coating were observed by scanning electron microscopy (SEM) with a ZEISS-LEO 1530 using the Inlense detector (Figure 13).

All tested mixing technologies leads, after process optimization, to what can be considered as a saturation of the host particles by the guest particles, whatever the particle size of the host particles.

355 The dry coating conforms to the host particles asperities observed in Figure 12-a. The very advanced covering is consistent with the Eq.(2) which set up for this study the saturation of the aluminium particle surface for 0.5 wt% of 35 nm guest particles. The SEM images of the nanocomposite powder prepared by acoustic mixing (Figure 13 –e) show less agglomerated guest particles onto the aluminium surface, which coatings that look “smoother”.

360 A higher powder friction (more inter-particle collisions) during acoustic mixing could explain an enhanced nanoparticle dispersion and pack density at host particle surface.



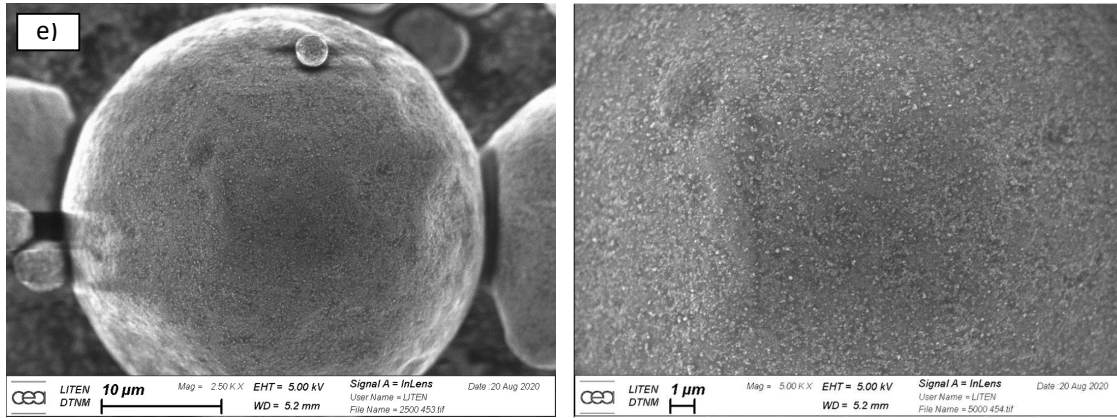


Figure 13: SEM images with magnification of 2500 (left) and 5000 (right). (a) Host aluminium powder and coated powder with 1wt% SiC 35nm using: (b) rotating drum mixer; (c) high shear paddle mixer, (d) low shear helices mixer; (e) acoustic mixer.

370

The automated image analysis of the particle morphology (Table 5) enables to detect possible plastic deformation of the product after mixing in statistically manner. As previously mentioned in section 3.1, the median aspect ratio of starting aluminium powder is close to 1 (0.91), meaning that the powder is highly spherical before mixing. A decrease of the median aspect ratio after mixing indicates a degradation of particle sphericity. Only the rotative drum mixing embedding grinding balls is lowering aspect ratio by crushing effect. Conversely, the higher energy mixers as high shear paddle mixer and acoustic mixer, applying only shearing forces or particle-to-particle frictions do not deform host particles.

375

	D10 ±0.02	D50 ±0.02	D90 ±0.02
AS7G06 initial host powder	0.69	0.91	0.98
Rotative drum coated Al powder	0.64	0.87	0.97
High shear paddle coated Al powder	0.71	0.92	0.98
Low shear helices coated Al powder	0.70	0.91	0.98
Acoustic coated Al powder	0.72	0.92	0.98

Table 5: Deciles of Al coated particles aspect ratio (width/length) measured by automated image analysis.

380

Lastly, the particle size reduction measured for the high shear paddle mixer (Figure 11) is not accompanied by a particle deformation. The shift in PSD observed previously would rather be the result of a higher de-agglomeration of host particles (less multi-particles sticking to each other) rather than a powder fracturing occurring during mixing.

385

After assessing the efficiency of the dry coating methods, the processability of the prepared nanocomposite powders for PBB-AM is discussed in the next section.

### 3.3 Assessment of nanocomposite powder processability

390

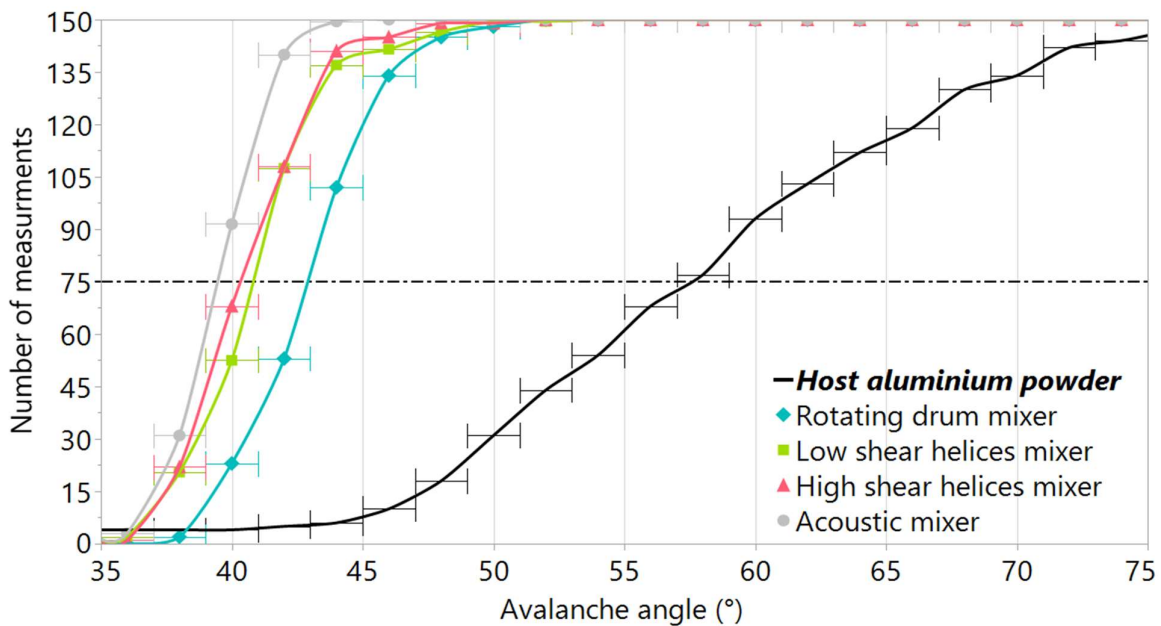
Flowability, apparent density and optical reflectivity properties of prepared nanocomposite powders were tested to track coating effect on host powder processability by L-PBF. A high powder free-flowability is recommended for L-PBF machines equipped with a hopper as powder feeding system. On the other hand, powder apparent density is highly correlated to the powder layer density spread in PBB-AM processes [2] [5] [12]. The powder optical absorption contributes to assess the powder-to-laser interaction. Increasing the powder optical absorption allows to reduce the required lasing energy to melt the powder bed and improve the process reliability [42].

395

The free-flowability of the different powder mixtures is assessed by avalanche angle measurements. (Figure 14). Corresponding median avalanche angles have been recorded in the Table 6, as well as Carney funnel measurements (5.0mm diameter orifice). The starting aluminium powder presents a very poor flowability, which translates into the absence of flow using the funnel test and a high median avalanche angle of 57.5°. Regardless of the coating process, the flowability of the nanocomposite Al/1wt% n-SiC powder is significantly improved in comparison with the aluminium powder alone. The composite powder avalanche angle is in the range of 39-43° and the time flow between 31 and 41 seconds, pointing out a clear drop in aluminium/aluminium particles cohesivity. The nanocomposite powder elaborated with the rotative drum mixer exhibits a slightly lower flowability compared to the others, which can be explained by the aluminium particles deformation measured by morphogranulometry during this mixing (Table 5).

400

405



410

Figure 14: Cumulative distributions of avalanche angles of coated aluminium powder using high shear paddle, rotative drum, low shear helices and acoustic mixers.

	AS7G06 initial host powder	AS7G06 / 1wt.% nano-SiC			
		Rotative drum mixer	High shear paddle mixer	Low shear helices mixer	Acoustic mixer
Median avalanche angle	57,5 ±1.1°	42,9 ±0.9°	40,3 ±0.8°	40,8 ±0.8°	39,5 ±0.8°
Sec/50g (Carney funnel)	No flow	39.5 ±1.1	41.5 ±0.5	37.0 ±0.9	31.0 ±0.6

Table 6: Median avalanche angle and time to flow in a Carney funnel of coated aluminium powders by 1wt.% of n-SiC.

415 From a general point of view, the as-coated Al powder exhibits an extremely high flowability with regard to the granulometry of the aluminium host powder. Indeed, the avalanche angles of dry coated aluminium powders are smaller than those of an uncoated aluminium powder having a coarser granulometry and an even more spherical particle shape (*Table 7*).

	AS7G06 / 1wt.% nano-SiC (Present work)			AS7G06 Powder 2 Uncoated		
	D50 (μm)	SPAN	Aspect ratio	D50 (μm)	SPAN	Aspect ratio
		31	1.1	0.91	45	0.7
Median avalanche angle	39.5-43°			47.2°		

420 *Table 7: Avalanche angle comparative of the SiC coated Al powder with an uncoated coarser and more spherical Al powder (measurments carried our under identical conditions).*

425 An interpretation of these findings is that the guest nanoparticles act as spacers between the aluminium particles reducing the Van der Waals attraction forces [32]. Indeed, Yang *et al.* [30] simplify the original Rumpf model to predict the amount of reduction in the cohesive force for the coated particles as follows:

$$\frac{F_{coated}}{F_{uncoated}} = \frac{d}{D} \quad \text{Eq. 3}$$

430 Where  $d$  is the diameter of guest nanoparticles and  $D$  is the host particles asperities estimated by Molerus *et al.* [43] at 0.2μm for micrometric particles. Even though an accurate measurement of the size of the asperities in the host powders is outside the scope of this paper, this 0.2 μm value appears qualitatively consistent with the SEM observations.

435 Moreover, an improvement of host powder flowability became significant from a  $d/D$  ratio close to 0.5 and further improved at 0.1 [30]. This present work makes use of an intermediate  $d/D$  ratio of 0.175 and is also consistent with the large reduction in the cohesive force in this range, with a ratio higher than 80% according to Eq. 3.

440 Moreover, these findings are also consistent with the results of the nanocomposite powder tapped and untapped densities measurements shown in *Table 8*, which indicate a higher degree of powder packing for coated powders compared to the initial aluminium powders. The results suggest that covering the aluminium surface with silicon carbide nanoparticles limits the cohesive forces between host particles (hydrogen bonds, Van der Waals forces).

	AS7G06 initial host powder	AS7G06 / 1wt.% nano-SiC			
		Rotative drum mixer	High shear paddle mixer	Low shear helices mixer	Acoustic mixer
Untaped/ Taped apparent density (g/cm <sup>3</sup> )	1.34 / 1.54	1.40 / 1.63	1.44 / 1.83	1.41 / 1.61	1.46 / 1.71

*Table 8: Apparent densities of coated Aluminium powders by 1wt.% of n-SiC.*

445 The impact of the dry coating on host powder reflectivity was assessed, in particular at 1064 nm, that corresponds to the wavelength of Nd:YAG laser equipping most of LPBF machines (*Figure 15*).

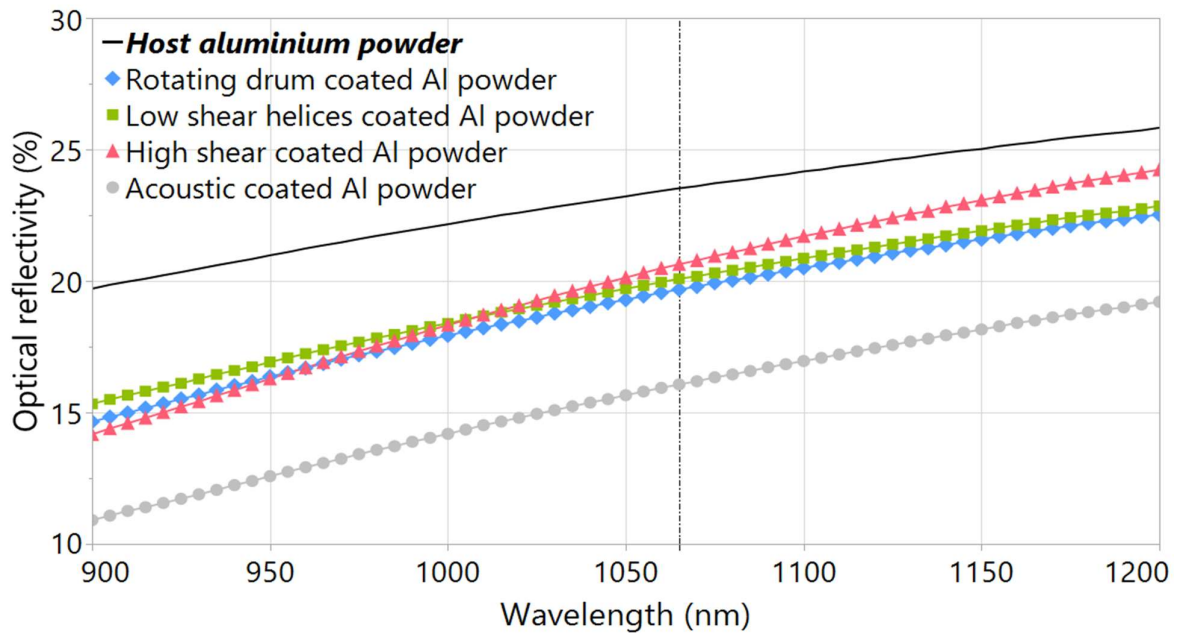


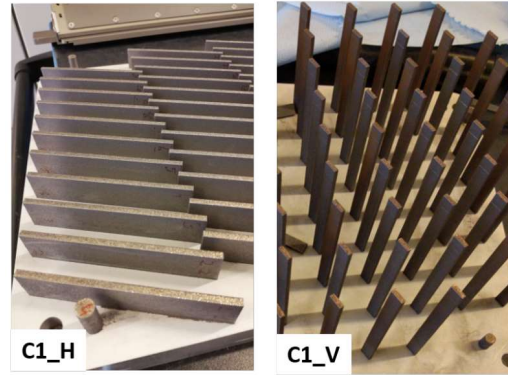
*Figure 15: Optical reflectivity of Al coated powder with 1wt% of n-SiC using high shear paddle, rotative drum, low shear helices and acoustic mixers.*

450 Surface coating of the aluminium powder leads to a decrease of its powder reflectivity all over the studied wavelength range (900-1200nm). At 1064 nm, the nanocomposite powder reflectivity varies from 16 to 20.5% depending on the coating process, as compared to 23.5% for the uncovered host powder. These substantial decreases of the powder reflectivity could be explained by the multiple internal reflections of the incoming laser light induced by the guest particles [42] [44].

455 The reflectivity of the powder treated in the acoustic mixer is lower than the others. The denser coating obtained with that mixer (*Figure 13-e*) reduces more efficiently the aluminium powder reflectivity. On the other hand, the resulting powder reflectivity after rotative drum, low shear and high shear mixing are conducting to similar values range, from 19.7% to 20.6%. These dry coating devices all conduct to an almost full surface coverage of aluminium host powder, which appears to drive the resulting optical  
460 absorption of the nanocomposite powders. The amount of SiC nanoparticles assembled at the host powder surface above the saturation point does not seem to impact the reflectivity measurements (let us recall that around 30 wt% of SiC nanoparticles are not coated with the low shear helices mixer, whereas the high shear paddle mixer ensure a complete electrostatic assembly of SiC nanoparticles). Analyses of the particle size distribution of the powder mixtures by morphogranulometry are more  
465 relevant to rank the dry mixers according to their respective coating efficiency (*Figure 11*).

In the frame of this study, the processability of uncoated and coated aluminium powder was assessed in a Laser Powder Bed Fusion SLM Solution® 280 HL machine equipped with a hopper feeding system. The uncoated aluminium powder leads to systematic hopper clogging, thus rendering not possible the spreading of powder layers. As stated above, this behavior is a consequence of the poor powder free-  
470 flowability measured by avalanche angle (*Figure 14*). The erratic flow through the feeding system does not occur when using the coated powder, prepared by rotative drum and high shear paddle mixers, resulting in good process control. Even though composite powders from the two other processes (acoustic and low shear mixers) were not evaluated in printing conditions, their similar properties

475 suggest a perfect compatibility also for these powders for the L-PBF process. These experimental evaluations in real conditions underline the high potential of powder dry coating to solve flow problems in printing machines hoppers. Finally, checks carried out on the laser melted nanocomposite powder shows the obtained material to be fully dense, with relative density measured by Archimedes' method higher than 99.5% (Figure 16).



480 Figure 16: Picture of tensile bars printed in SLM Solution® L-PBF system (model 280 HL) using dry coated Al/SiC 1wt% powder prepared by high shear mixer.

### 3.4 Effect of guest particle oxidation on dry coating efficiency

485

Dry particle coating is the result of electron transfer through the surfaces of dissimilar particles [45]. Polarity and charging amount is governed by the electron donor-acceptor properties of species composing the surface of the host and guest particles [46] [47]. Thus, a particle surface oxidation can affect the dry coating efficiency. Shimoda *et al.* pointed out that different commercial SiC nanopowders can feature various surface compositions depending on their production method (Laser pyrolysis, CVD, PE-CVD etc...)[48]. Starting Nanomakers powder surface is free of oxide layer, whereas other products could present at their surface either siliconoxycarbide species ( $\text{SiO}_x\text{C}_y$ ), silicon oxide ( $\text{SiO}_{2-x}$ ), silica ( $\text{SiO}_2$ ) or a combination of them. Moreover, the storage conditions of powders can obviously affect the surface species post-production, and potentially alter the reproducibility of the tribo-charging.

495

The effect of a pre-oxidation of SiC nanoparticles on dry coating efficiency was studied by heat-treating Nanomakers SiC nanoparticles in air at 850°C for 2 hours. The surface chemical bond of SiC nanoparticles were analyzed before and after oxidation by X-ray photoelectron spectroscopy (XPS). Figure 17 shows the spectra of Si 2P-based bonds (Binding energy =110-95 eV), with a depth analysis on the order of 5nm. The corresponding atomic percent based on the O 1s, C 1s and Si 2p signals determined for the surface of SiC nanopowders are given in Table 9. Initial SiC nanopowders produced by laser pyrolysis present a high purity with a main peak corresponding to Si-C bond at binding energy of 100.0 eV and a the lower intensity peak at higher binding energies (101.2 eV) consisting of a siliconoxycarbide impurity ( $\text{Si-O}_x\text{-C}_y$ ). The relative intensity of the  $\text{Si-O}_x\text{-C}_y$  to Si-C bonds allow estimating the  $\text{Si-O}_x\text{-C}_y$  layer thickness at 1 nanometer. These results are in good agreement with the previous work of Shimoda *et al.* characterizing the surface properties of SiC produced by Nanomakers [48]. After heat treatment, an intense peak corresponding to  $\text{SiO}_2$  at the binding energy of 102.7eV is detected at the expense of the Si-C bond and  $\text{Si-O}_x\text{-C}_y$  bond. The thickness of the silica layer is estimated to be 3-4 nanometers by the relative peak intensities  $\text{SiO}_2$  peak and Si-C peak (the depth analysis of these XPS is ~ 5 nm).

510

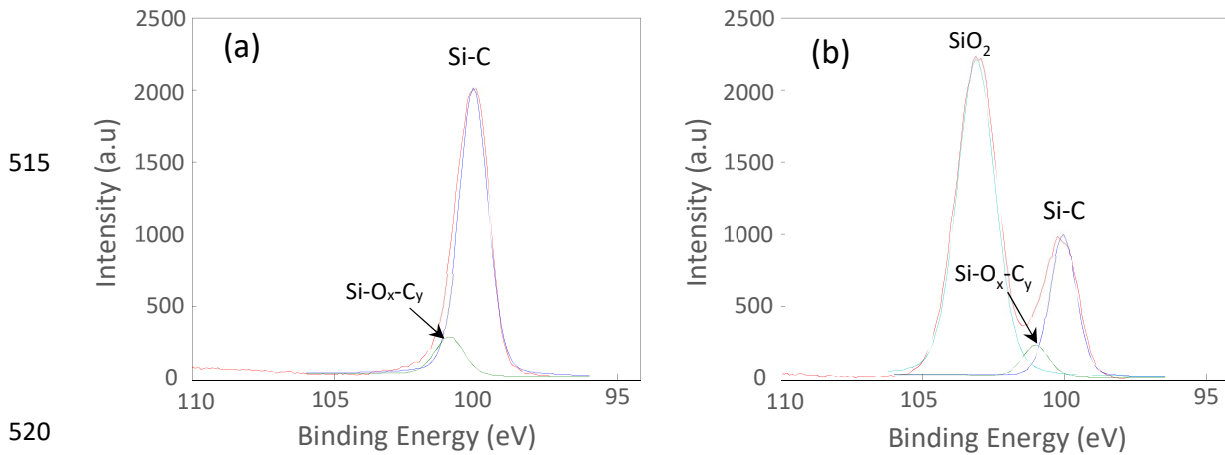


Figure 17: XPS spectra of Si 2p peak or (a) starting SiC nanoparticles and (b) after air oxidation at 850°C during 2 hours.

	Si (at.%)	O (at.%)	C (at.%)
Initial SiC	59	4	37
Oxidized SiC at 850°C 2h	19	48	33

Table 9: Semi-quantitative chemical analysis of the extreme surface of the SiC nanoparticles by XPS.

525

Dry mixing experiments of pre-oxidized SiC nanoparticles were conducted with acoustic mixer and rotative drum mixers, without changing the optimized mixing parameters previously identified. The PSD analysis presented in Figure 18 shows a very uncomplete electrostatic assembly of pre-oxidized SiC using the rotative drum mixer, whereas the impact of oxidation on the coating efficiency is reduced using acoustic mixing. As shown in Figure 19-a, the former mixer leads to partially uncoated aluminium particles and high agglomeration of SiC at the aluminium surface, which look like patches. Conversely, a continuous coating of oxidized SiC nanoparticles is achieved on the majority of aluminium particles using the acoustic mixer (Figure 19-b). However, the coating appears less uniform and rougher compared to the coatings obtained with unoxidized SiC (Figure 13-e), because of a higher degree of SiC agglomeration at the surface of host particles.

530  
535

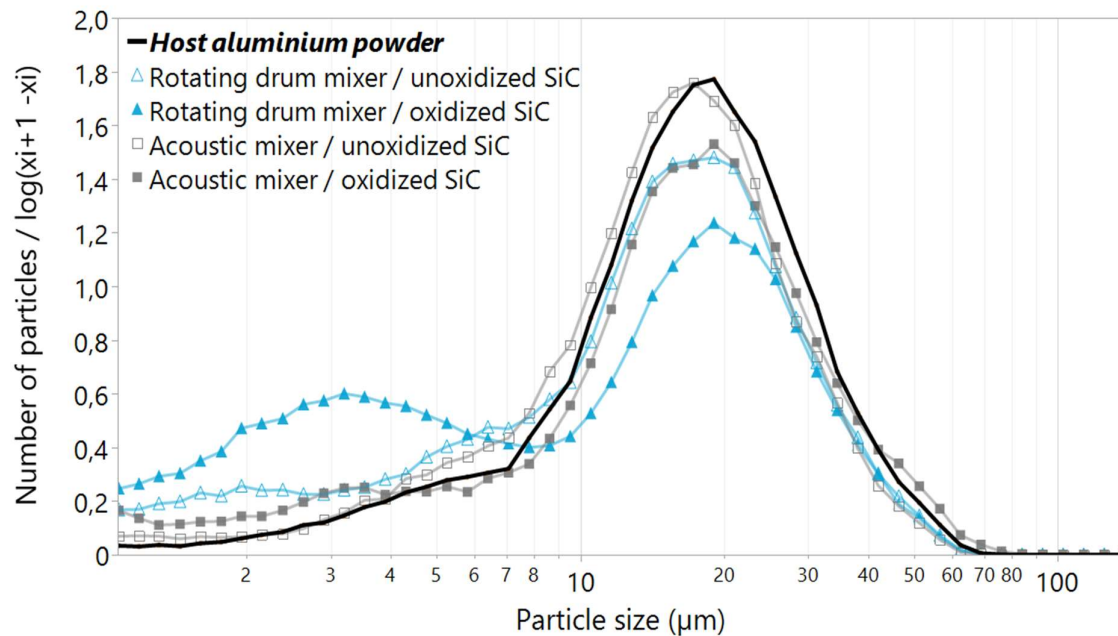


Figure 18: Effect of a SiC pre-oxidation on the PSD of Al/SiC mixture using rotative drum mixer and acoustic mixer. PSD evaluations are performed by automated image analysis.

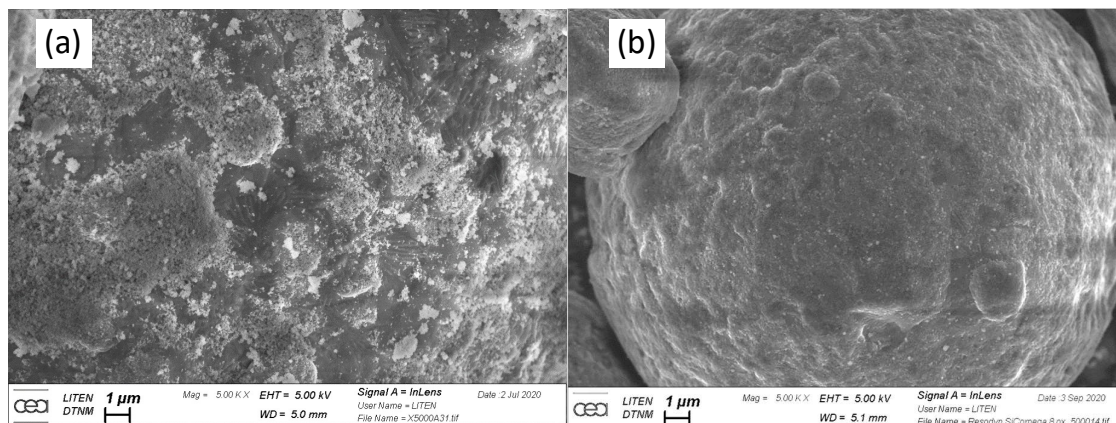


Figure 19: SEM images of coated aluminium with 1wt% of pre-oxidized SiC nanoparticles. (a) Rotative drum dry coating; (b) Acoustic dry coating.

545 These results point out the significant effect of a guest surface oxidation level on the coating efficiency. To predict the polarity of an oxide material in contact to a metal material, Ogushi *et al.* [47] established a relation between the charging tendency and the acido-basic properties of the oxide material. In particular, the silica material here covering the SiC nanoparticles, as an oxide of acidic metal (Si) present a negative charging tendency when contact is made with aluminium material. Ogushi *et al.*  
 550 explains this tendency by the higher Pauling electronegativity of silicon compared to aluminium ( $\chi_{Si} = 1.9$ ,  $\chi_{Al} = 1.6$ ) and a resulting higher electron attractive power. Despite this polarity, the absence of particle self-assembly between oxidized SiC and aluminium reveals an insufficient charging amount to ensure a complete dry coating. Matsusaka *et al.* (2000) and Matsuyama *et al.* (2006) have respectively

555 experimented and simulated the charge accumulation of powder according to repeated impacts [49][50]. The present study underlines that high-energy mixers like acoustic mixer, involving high particle friction and collisions are more adapted to maximize particle charging and facilitate particles self-assembly thus being more tolerant to potential oxidation of starting powders.

## 4. Conclusions

560 The objective of the present work is to assess the potential of dry coating to elaborate nanocomposite powder for powder bed based (PBB) additive manufacturing. The selected case study consists in dry coating an aluminium alloy powder (AS7G06, 15-53  $\mu\text{m}$ ) by nanosized silicon carbide particles (35 nm), using a panel of devices covering different mixing energy ranges, from rotative drum to high shear paddle and acoustic mixers.

565 All dry coating devices lead to an almost total coverage of the surface of host particles using 1 wt% of SiC nanoparticles. The experimental results agree with the theoretical prediction estimating a complete surface saturation for 0.5 wt% of guest particles.

570 If electrostatic assembly is effective for all mixers, the low energy mixers tested which are rotative drum mixer and low shear mixer conduce to longer operating time and not allow a complete dispersion of nano-silicon carbide agglomerates. Consequently, the resulting powder mixtures remains unstable, embedding free flowing silicon carbide agglomerates prone to segregation within the mixture during transport, powder handling or processing. This result points out the two quite distinct steps occurring during a dry coating; a first deagglomeration of guest SiC nanoparticles and their assembly to host particle surfaces by triboelectricity. The rotative drum mixer, as a convection mixer, is applying a large-scale movement of powder is poorly adapted to dry coating. Addition of milling balls in this configuration allow a better SiC dispersion but deforms the starting aluminium powder.

575 Shearing forces generated by the helices of the low shear mixer, rotating at 2 m/s tangential speed, appears again not sufficient as at least 30% of starting SiC nanoparticles remain in free form in the final powder mixture.

580 Acoustic mixer and high shear paddle mixer appear to be the most suitable mixers for the size reduction of silicon carbide agglomerates, dispersion and assembly of nanoparticles onto host aluminium particles thanks to electronic transfer between host and guest particles. These technologies lead to fully coated host particles with nanosized guest particles ensuring the stability of the powder mixture elaborated. They are capable of near-field particles rearrangement either by particle-to-particle friction or by high shear forces of paddles rotating at high tangential speed ( $>10$  m/s). Besides, these high-energy mixing devices do not deform plastically ductile host particles.

590 Powder flowability of dry coated aluminium powder points out a clear improvement compared to the uncoated powder, whatever the coating device. This result is in agreement with the simplified Rumpf model proposed by Yang *et al.* predicting a decrease of more than 80% of the cohesive forces using 35 nm guest particles. The overall processability of the dry coated aluminium is enhanced for powder-bed-based additive manufacturing, improving also the powder packing (apparent density) and optical reflectivity of the host powder, another interesting feature for laser melting process.

595 Surface oxidation of the guest SiC particles has a great impact on the coating efficiency of aluminium powders. The reproducibility of the electrostatic coating appears to be more reliable and less dependent on the particle surface state using a high-energy mixer. High particle-to-particle friction promote charge accumulation and stability of the prepared nanocomposite powders.

To further understand the mechanisms of electrostatic self-assembly, it could be interesting to use the blow-off method in order to measure the amount of electric charge accumulated according to the used

600 coating devices and the composition of the guest particles. The principle is to separate in a Faraday cage the guest and host particles by a flux of compressed nitrogen. The guest particles are blown-out the Faraday cage, and the host particles kept in the cage by a filter becomes charged. This charge is collected by the cage and measured by an electrometer [47].

605 This work proposes a methodology to assess the dry coating efficiency and optimize the processing time by following the powder mixture morphogranulometry. We show also that powder functionalization by dry particle coating has a high potential for PBB-AM to prepare stable powder mixtures and to improve all at the same time powder flowability, powder packing, while adding nanosized reinforcements in a metallic powder. Dry coating also offers an opportunity to reduce significantly the host powder reflectivity from a laser source (special interest for laser melting process) or increase the sinterability by adding nanosized particles more reactive during sintering (interest for binder jetting technology).

610  
615 Another development perspective is to reduce the powder costs by converting initially unsuitable powder for additive manufacturing (fine and cohesive powders) into a spreadable powder by dry coating the initial powder with nano sized flow aids. Regarding health concerns, the interactive mixing makes able to incorporate nanoparticles while limiting the exposure to nanomaterials by inhalation or ingestion.

## 5. Acknowledgments

620 This work was founded by EIT Raw Materials, supported by the EIT, a body of the European Union. The HIPERCO project (High PERFORMANCE COMposite based on aluminium) is embedding a consortium covering the complete process chain of metal additive manufacturing from the powder atomization to the printing of Al/SiC nanocomposite parts for airplane applications. The XPS experiments were made possible through the Nano-Characterisation Platform (PFNC) at Minatec/France. Thanks are due to J.P. Garandet for his help in improving the presentation of the manuscript.

## 6. References

- 630 [1] L. Hitzler *et al.*, A Review of Metal Fabricated with Laser- and Powder-Bed Based Additive Manufacturing Techniques: Process, Nomenclature, Materials, Achievable Properties, and its Utilization in the Medical Sector, *Advanced Engineering Materials*, 20 (2018). <https://doi.org/10.1002/adem.201700658>.
- [2] M. Ziaee *et al.*, Binder jetting: A review of process, materials, and methods, *Additive Manufacturing* 28 (2019) 781–801. <https://doi.org/10.1016/j.addma.2019.05.031>
- 635 [3] A.B. Spiering *et al.*, Powder flowability characterisation methodology for powder-bed-based metal additive manufacturing, *Prog. Addit. Manuf.* 1, (2016) 9–20. <https://doi.org/10.1007/s40964-015-0001-4>.
- [4] X. Jia *et al.*, A packing algorithm for particles of arbitrary shapes, *Powder Technology* 120 (2001) 174-186. [https://doi.org/10.1016/S0032-5910\(01\)00268-6](https://doi.org/10.1016/S0032-5910(01)00268-6)
- 640 [5] M. Soulier *et al.*, Analytical and Numerical Modelling of Stainless Steel Powders Spreading in Powder-Bed Processes for Additive Manufacturing, Conference paper Euro PM 2021.
- [6] C. Meier *et al.*, Critical influences of particle size and adhesion on the powder layer uniformity in metal additive manufacturing, *Journal of Materials Processing Technology* 266 (2019) 484-501. <https://doi.org/10.1016/j.jmatprotec.2018.10.037>
- 645 [7] K. Marchais *et al.*, A 3D DEM simulation to study the influence of material and process parameters on spreading of metallic powder in additive manufacturing, *Computational Particle Mechanics* 8 (2021) 943-953. <https://doi.org/10.1007/s40571-020-00380-z>

- 650 [8] G-C Cho *et al.*, Particle Shape Effects on Packing Density, Stiffness, and Strength: Natural and Crushed Sands, *Journal of Geotechnical and Geoenvironmental Engineering* 132(5) (2006) 591-602. [10.1061/\(ASCE\)1090-0241\(2006\)132:5\(591\)](https://doi.org/10.1061/(ASCE)1090-0241(2006)132:5(591))
- [9] A. Anand *et al.*, Predicting discharge dynamics from a rectangular hopper using discrete element method (DEM), *Chemical Engineering Science* 63 (2008) 5821—5830. [10.1016/j.ces.2008.08.015](https://doi.org/10.1016/j.ces.2008.08.015)
- 655 [10] N. Vlachos *et al.*, Investigation of flow properties of metal powders from narrow particle size distribution to polydisperse mixtures through an improved Hall-flowmeter, *Powder Technology* 205 (2001) 71-80. <https://doi.org/10.1016/j.powtec.2010.08.067>
- [11] E. Vasquez *et al.*, Effect of powder characteristics on production of oxide dispersion strengthened Fe- 14Cr steel by laser powder bed fusion, *Powder Technology* 360 (2020) 998–1005. <https://doi.org/10.1016/j.powtec.2019.11.022>
- 660 [12] M. Soulier *et al.*, Study of 316L stainless steel powders specifications on parts printed by laser-powered -powder bed fusion (PBF), Conference paper Euro PM 2018.
- [13] M. Soulier *et al.*, Analytical And Numerical Modeling Of Stainless Steel Powders Spreading In Powder-Bed Processes For Additive Manufacturing, Conference paper Euro PM 2021.
- 665 [14] S. Yadav *et al.*, Micro/Nano Reinforced Filled Metal Alloy Composites: A Review Over Current Development in Aerospace and Automobile Applications, *Materials Today: Proceedings* 4 (2017) 5571–5582. <https://doi.org/10.1016/j.matpr.2017.06.014>.
- [15] X. Li *et al.*, Theoretical and experimental study on ultrasonic dispersion of nanoparticles for strengthening cast aluminum alloy A356, *Journal of Metallic Science and Technology* 26-2 (2008) 112-120.
- 670 [16] B. Chen *et al.*, Recent progress in laser additive manufacturing of aluminium matrix composites, *Current Opinion in Chemical Engineering*, 28 (2020) 28–35. <https://doi.org/10.1016/j.coche.2020.01.005>.
- [17] D. Gu *et al.*, Rapid fabrication of Al-based bulk-form nanocomposites with novel reinforcement and enhanced performance by selective laser melting, *Scripta Materialia* 96 (2015) 25–28. <https://doi.org/10.1016/j.scriptamat.2014.10.011>.
- 675 [18] Li *et al.*, Laser Additive Manufacturing on Metal Matrix Composites: A Review, *Chinese Journal of Mechanical Engineering* (2021) 34-38. <https://doi.org/10.1186/s10033-021-00554-7>
- 680 [19] D.E. Cooper *et al.*, Additive layer manufacture of Inconel 625 metal matrix composites, reinforcement material evaluation, *Journal of Materials Processing Technology* 213 (2013) 2191-2200. [10.1016/j.jmatprotec.2013.06.021](https://doi.org/10.1016/j.jmatprotec.2013.06.021)
- [20] Z. Zhang *et al.*, Consideration of Orowan strengthening effect in particulate-reinforced metal matrix nanocomposites: A model for predicting their yield strength, *Scripta Materialia* 54 (2006) 1321-1326. <https://doi.org/10.1016/j.scriptamat.2005.12.017>
- 685 [21] R. Casati *et al.*, Metal Matrix Composites Reinforced by Nano-Particles—A Review, *Metals* 4 (2014) 65-83. [doi:10.3390/met4010065](https://doi.org/10.3390/met4010065)
- [22] M. Opprecht *et al.*, A solution to the hot cracking problem for aluminium alloys manufactured by laser beam melting, *Acta Materialia* 197 (2020) 40-53. <https://doi.org/10.1016/j.actamat.2020.07.015>
- 690 [23] J.H. Martin *et al.*, 3D printing of high-strength aluminium alloys, *Nature* 549 (2017) 365-369. <https://doi.org/10.1038/nature23894>.
- [24] A. Madian *et al.*, Impact of fine particles on the rheological properties of uranium dioxide powders, *Nuclear Engineering and Technology* 52 (2020) 1714-1723. [10.1016/j.net.2020.01.012](https://doi.org/10.1016/j.net.2020.01.012)
- 695 [25] J.N. Israelachvili, *Intermolecular and Surface Forces*, Academic Press, London, 1991. <https://doi.org/10.1016/C2009-0-21560-1>
- [26] J.P.K. Seville *et al.*, Interparticles forces in fluidisation: a review, *Powder Technology* 113 (2000) 261-268. [10.1016/S0032-5910\(00\)00309-0](https://doi.org/10.1016/S0032-5910(00)00309-0)

- 700 [27] K. Traina *et al.*, Flow abilities of powders and granular materials evidenced from dynamical tap density, Powder Technology 235 (2013) 842-852. <https://doi.org/10.1016/j.powtec.2012.11.039>
- [28] C. Suryanarayana, Mechanical alloying and milling, Progress in Materials Science 46 (2001) 1-184. [https://doi.org/10.1016/S0079-6425\(99\)00010-9](https://doi.org/10.1016/S0079-6425(99)00010-9)
- 705 [29] R. Pfeffer *et al.*, Synthesis of engineered particulates with tailored properties using dry particle coating, Powder Technology 117 (2001) 40-67. [https://doi.org/10.1016/S0032-5910\(01\)00314-X](https://doi.org/10.1016/S0032-5910(01)00314-X)
- [30] J. Yang *et al.*, Dry particle coating for improving the flowability of cohesive powders, Powders Technology 158 21-33 (2005). <https://doi.org/10.1016/j.powtec.2005.04.032>
- 710 [31] L-P Lapierre-Boire *et al.*, Improvement of flow of an iron-copper-graphite powder mix through additions of nanoparticles, Powder Technology 299 (2016) 156-167. <https://doi.org/10.1016/j.powtec.2016.05.046>
- [32] H. Rumpf, Die Wissenschaft des Agglomerierens, Chemie-Ingenieur-Technik 46 (1974) 1– 11. <https://doi.org/10.1002/cite.330460102>.
- 715 [33] M. Soulier *et al.*, Z3DLAB SAS, Additive manufacturing of composite materials Titanium / Zirconium, 20èmes Assises Européennes de Prototypage Rapide (2015).
- [34] Z. Huang *et al.*, Flow and bulk density enhancements of pharmaceutical powders using a conical screen mill: A continuous dry coating device, Chemical Engineering Science 125 (2015) 209–224. <https://doi.org/10.1016/j.ces.2014.05.038>
- 720 [35] S. Chattoraj *et al.*, Profoundly improved flow properties of a cohesive cellulose powder by surface coating with nano-silica through comilling, Journal of Pharmaceutical Sciences 100-11 (2011) 4943-4952. <https://doi.org/10.1002/jps.22677>
- [36] M. Ramlakhan *et al.*, Dry particle coating using magnetically assisted impaction coating: modification of surface properties and optimization of system and operating parameters, Powder Technology 112 (2000) 137-148. [https://doi.org/10.1016/S0032-5910\(99\)00314-9](https://doi.org/10.1016/S0032-5910(99)00314-9)
- 725 [37] J.G. Osorio *et al.*, Evaluation of resonant acoustic mixing performance, Powder Technology 278 (2015) 46-56. <https://doi.org/10.1016/j.powtec.2015.02.033>
- [38] S. Otles *et al.*, Dry particle high coating of biopowders: An energy approach, Powder Technology 208 (2011) 378-382. <https://doi.org/10.1016/j.powtec.2010.08.032>
- 730 [39] W.D. Greason *et al.*, Investigation of a test methodology for Triboelectrification, Journal of Electrostatics 49 (2020) 245-256. [https://doi.org/10.1016/S0304-3886\(00\)00013-9](https://doi.org/10.1016/S0304-3886(00)00013-9).
- [40] T. Nomura *et al.*, The environment humidity effect on the tribo-charge of powder, Powder Technology 135/136 (2003) 216-222. [https://doi.org/10.1016/S0032-5910\(03\)00157-8](https://doi.org/10.1016/S0032-5910(03)00157-8).
- [41] J. J. Dunkley, C. Schade, Atomization in: P. Samal and J. Newkirk (Eds.), Powder Technology, ASM Handbook Volume 7, 2015, pp58-71.
- 735 [42] S.D. Jadhav *et al.*, Mechanical and electrical properties of selective laser-melted parts produced from surface oxidized copper powder, Material Design & Processing Communications e94, vol. 2 (2020). <https://doi.org/10.1002/mdp2.94>.
- [43] O. Molerus *et al.*, The role of science in particle technology, Powder Technology 122 (2002) 156-167. [https://doi.org/10.1016/S0032-5910\(01\)00412-0](https://doi.org/10.1016/S0032-5910(01)00412-0).
- 740 [44] P. Lassègue *et al.*, Laser powder bed fusion (L-PBF) of Cu and CuCrZr parts: Influence of an absorptive physical vapor deposition (PVD) coating on the printing process, Additive Manufacturing 39 (2021) 101888. <https://doi.org/10.1016/j.addma.2021.101888>
- [45] W.R. Harper, The Volta effect as a cause of static electrification in: G. Thomson, FRS (Eds.), J. Dunkley, C. Schade, Atomization in: P. Samal and J. Newkirk (Eds.), 1951, pp83-102. <https://doi.org/10.1098/rspa.1951.0019>.
- 745 [46] S. Matsusaka *et al.*, Triboelectric charging of powders: A review, Chemical Engineering Science 65 (2010) 5781–5807. <https://doi.org/10.1016/j.ces.2010.07.005>.
- [47] T. Oguchi *et al.*, Contact Electrification in Inorganic Binary Compounds, Journal of The Electrochemical Society, 133 (1986) 841-847.

- 750 [48] K. Shimoda *et al.*, Surface properties and dispersion behaviors of SiC nanopowders, *Colloids and Surfaces A: Physicochem. Eng. Aspects* 463 (2014) 93–100. <https://doi.org/10.1016/j.colsurfa.2014.09.013>.
- [49] S. Matsusaka *et al.*, Electrification of an elastic sphere by repeated impacts on a metal plate, *Journal of Physics D: Applied Physics* 33 (2000) 2311-2319. <https://doi.org/10.1088/0022-3727/33/18/316>.
- 755 [50] T. Matsuyama *et al.*, Montecarlo simulation of charge accumulating process of a single particle due to successive impacts, *Journal of the Society of Powder Technology, Japan* 43 (2006) 169-173.